# Electronic Supplementary Material

## Selective $CO_2$ or $CH_4$ Adsorption of Two Anionic *bcu*-MOFs with Two Different Counterions: Experimental and Simulation Studies

Qian Wang*[a,†], Liuli Meng[a,†], Hongtao Cheng[a], Zonghui Zhang[a], Dongxu Xue[a], and Junfeng Bai*[a,b]

[a] *Key Laboratory of Applied Surface and Colloid Chemistry, Ministry of Education, School of Chemistry & Chemical Engineering, Shaanxi Normal University, Xi'an 710062, PR China*

[b] *State Key Laboratory of Coordination Chemistry, School of Chemistry & Chemical Engineering, Nanjing University, Nanjing 210093, PR China*

**General procedures.** All reagents were obtained from commercial vendors and, unless otherwise noted, were used without further purification. Elemental analysis (C, H, N) were carried out with an Elementar Vario EL III. The IR spectra were obtained in the 4000~400 $cm^{-1}$ on a Bruker Tensor27 spectrometer using KBr pellets. Thermal gravimetric analyses (TGA) were performed under $N_2$ atmosphere (100 ml/min) with a heating rate of 5 °C/min using a Beijing Henven HTG-1 thermogravimetric analyzer. Powder X-ray diffraction (PXRD) data were collected on a Bruker D8 ADVANCEX-ray diffractometer with Cu Kα radiation. The content of Cu, Li and Fe in MOF sample was carried out with Optima 5300 DV ICP.

***Table S1.*** Crystallographic Data of SNNU-Bai66

| **MOF** | **SNNU-Bai66** |
|---|---|
| Empirical formula | $C_{34}H_{32}ClCu_4N_{17}O_{12}$ |
| Formula weight | 1135.18 |
| T [K] | 153(2) |
| Wavelength [Å] | 0.71073 |
| Crystal system | Tetragonal |
| Space group | *I4/mmm* |
| a [Å] | 13.3835(5) |
| b [Å] | 13.3835(5) |
| c [Å] | 20.4367(15) |
| α [deg] | 90 |
| β [deg] | 90 |
| γ [deg] | 90 |
| V [Å$^3$] | 3660.6(4) |
| Z | 2 |
| $\rho_{calc}$[g cm$^{-3}$] | 1.030 |
| $\mu$ [mm$^{-1}$] | 1.230 |
| F(000) | 1118 |
| Crystal size [mm$^3$] | 0.21 × 0.18 × 0.15 |
| Theta range [deg] | 2.934 − 24.125 |
| Limiting indices | -13 < = h < = 15 |
| | -15 < = k < = 14 |
| | -23 < = l < = 23 |
| Reflections collected | 5856 |
| Reflections unique | 862 [R(int) = 0.0264] |
| Completeness | 97.8 % |
| Data/restraints/parameters | 862 / 5 / 64 |
| Goodness-of-fit on F^2 | 1.077 |
| R1, wR2[a] [I>2σ(I)] | 0.0732, 0.2161 |
| R1, wR2[a][all data] | 0.0737, 0.2166 |
| $\Delta\rho_{max}$ / $\Delta\rho_{min}$[e. Å$^{-3}$] | 2.504 / -0.708 |

[a] $R1 = \Sigma||F_o| - |F_c||/|F_o|$; $wR2 = [\Sigma w(\Sigma F_o^2 - F_c^2)^2/\Sigma w(F_o^2)^2]^{1/2}$.

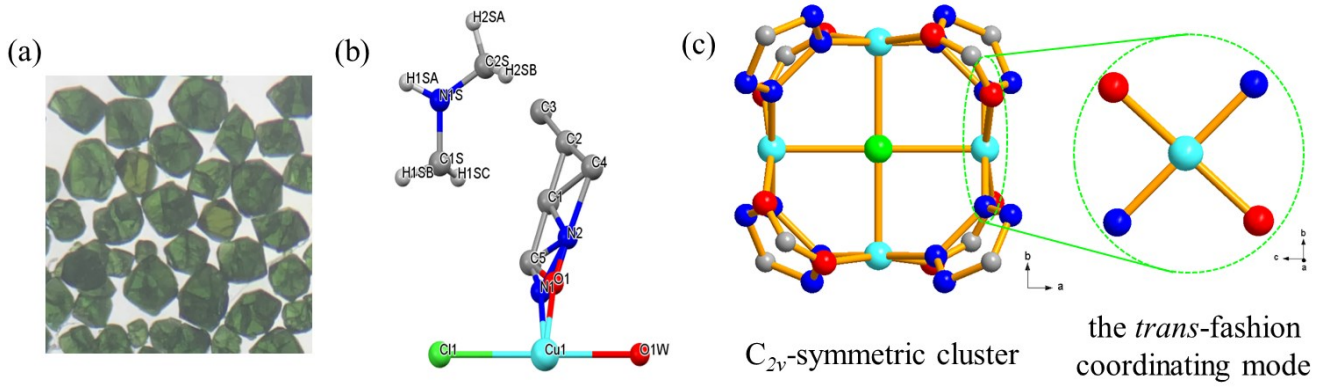


***Figure S1.*** (a) the optical microscope image of green crystals of SNNU-Bai66; (b) the asymmetric unit of SNNU-Bai66; (c) the *trans*-fashion coordinating mode of N and O atoms onto each $Cu^{2+}$ ion in the $C_{2v}$-symmetric $[Cu_4Cl(COO)_4N_8]$ cluster of SNNU-Bai66.

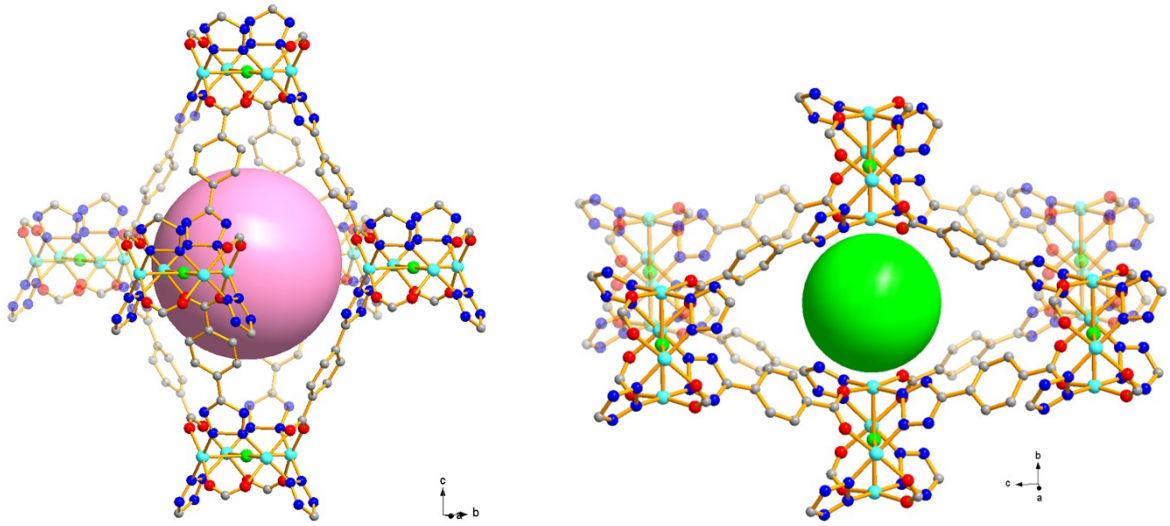


***Figure S2.*** The $C_4$-symmetric elongated equatorial plane-unedged octahedron cage A (a) and $C_4$-symmetric flaser equatorial plane-unedged octahedron cage B (b) in SNNU-Bai66. H atoms have been omitted for clarity.

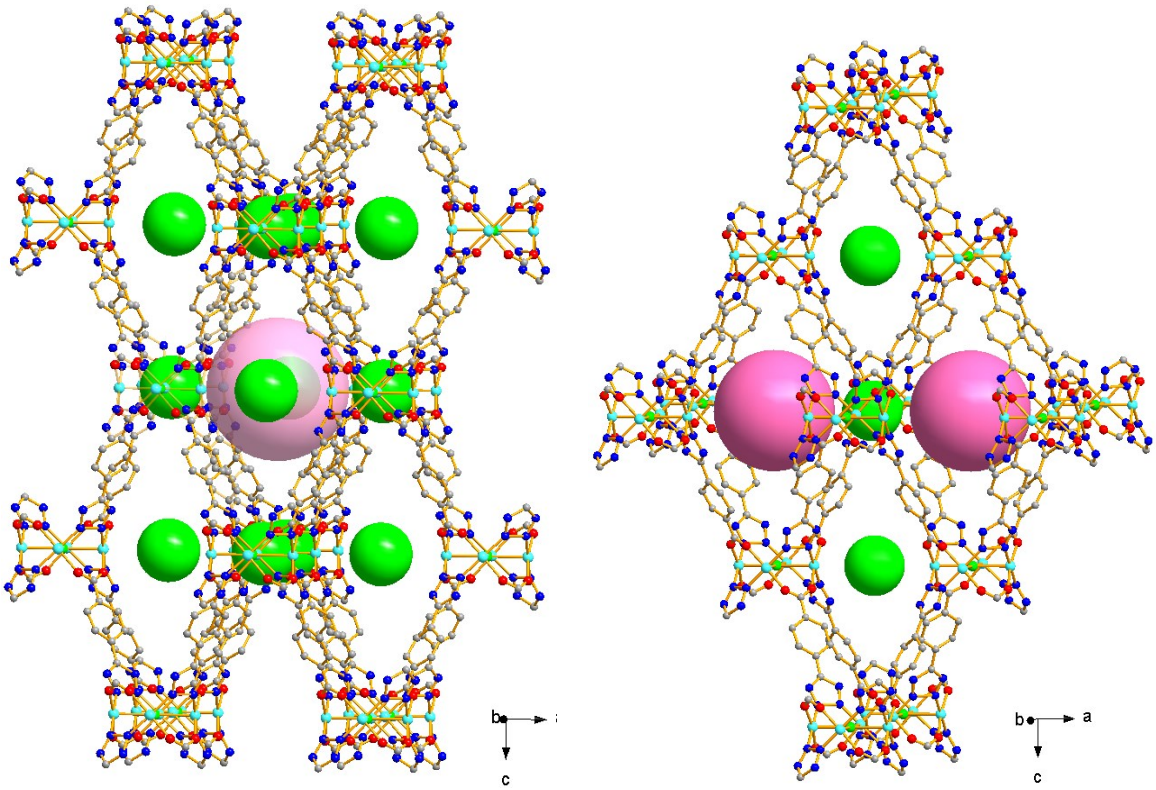


(a) (b)

***Figure S3.*** The surround environment of cage A with twelve cages B arranged through sharing their faces (a) and that of cage B with two cages A and two cages B arranged by sharing their faces (b) in SNNU-Bai66.

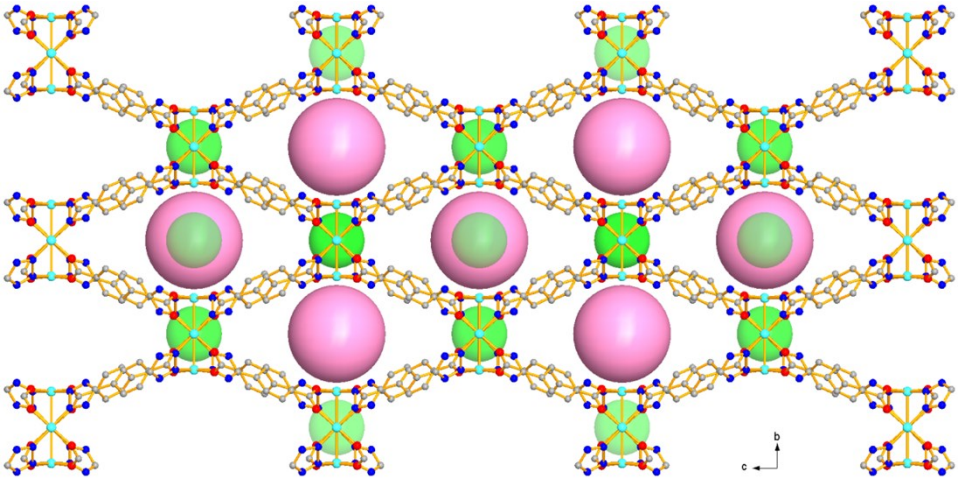


(a)

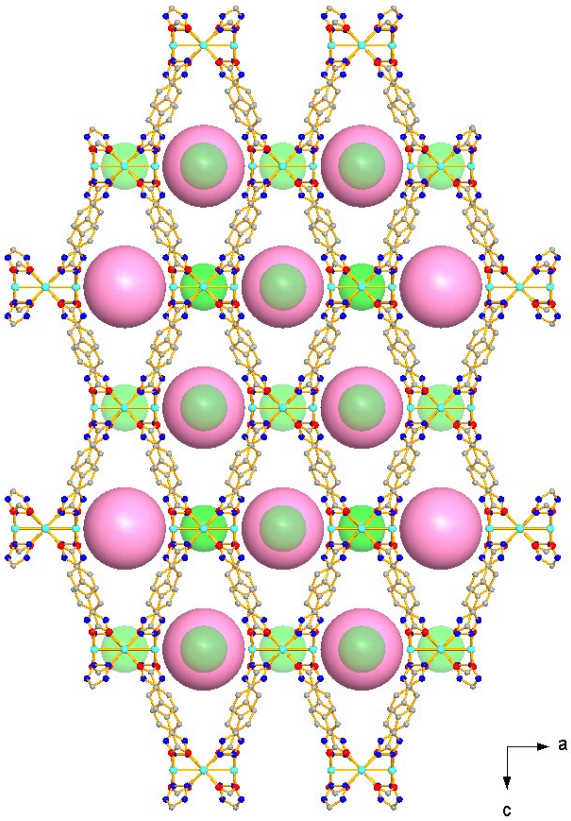


(b)

***Figure S4.*** The 3D structure viewed along **a** (a) and **b** axis (b) in SNNU-Bai66.

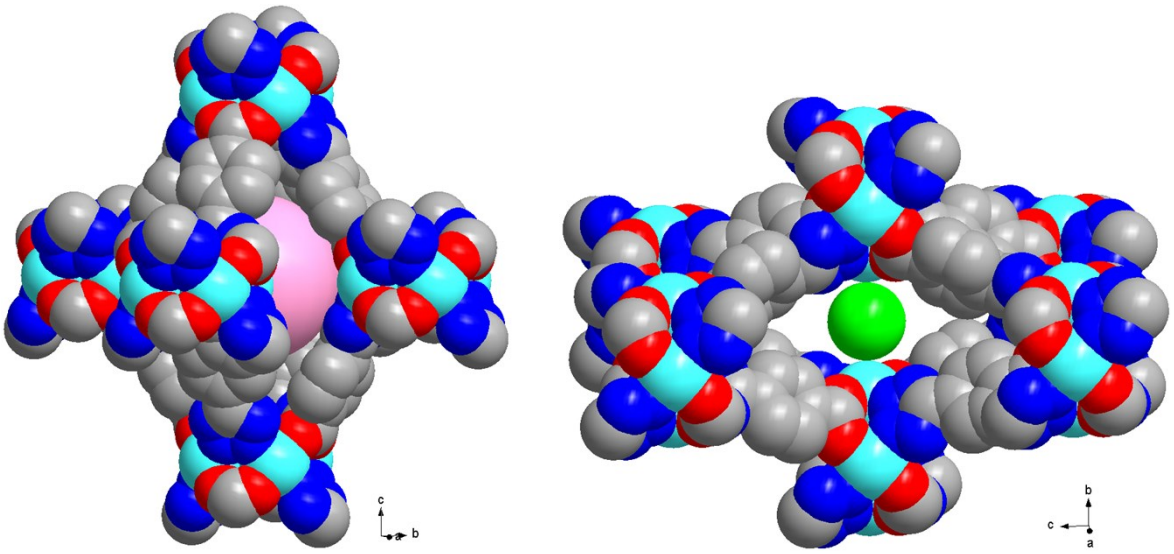

(a) (b)

***Figure S5.*** The pore sizes of cage A (a) and cage B (a) in SNNU-Bai66.

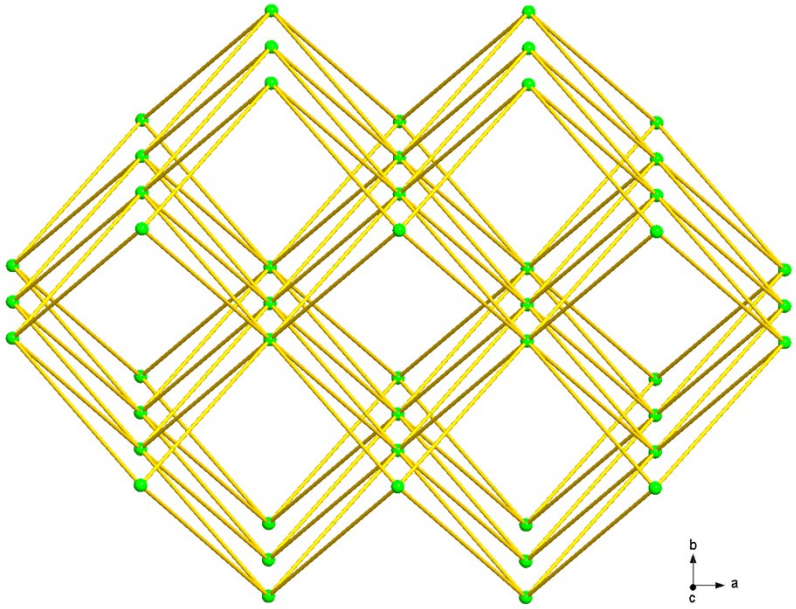

***Figure S6.*** The 3D **bcu**-topological net with point symbol of $\{4^{24}.6^{4}\}$ viewed along **c** axis in SNNU-Bai66.

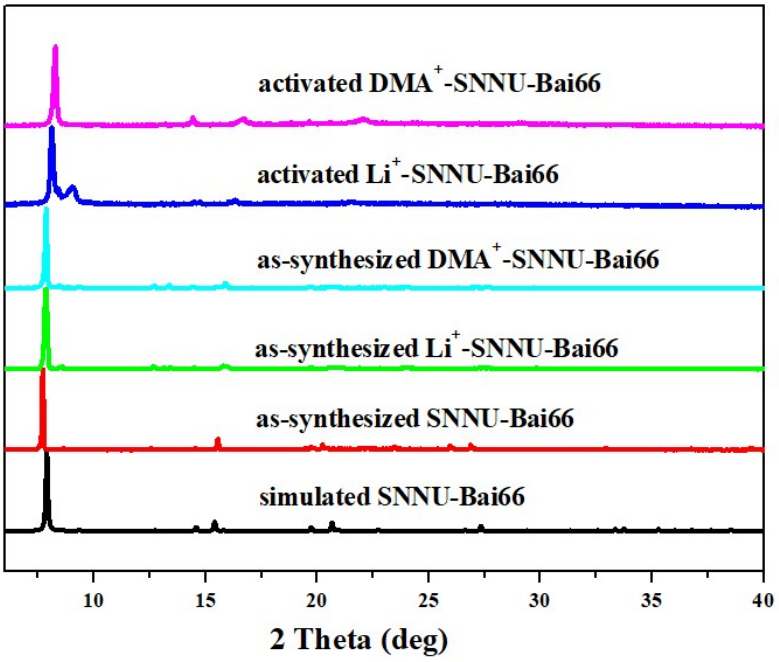


***Figure S7.*** The PXRD patterns of $Li^+$-SNNU-Bai66 and $DMA^+$-SNNU-Bai66.

The thermogravimetric analysis (TGA) of SNNU-Bai66 was measured to investigate the thermal stability. In the TGA plots, the as-synthesized SNNU-Bai66 takes place the first weight-loss around 75 ℃, which is corresponding to the loss of MeOH molecules packed in the pores, and then takes place the second weight-loss around 175 ℃, which is attributed to the loss of DMF molecules packed in the pores and the coordinated water molecules on $Cu^{2+}$ ions. Subsequently, the framework of as-synthesized SNNU-Bai66 occurs to partially collapse around 200 ℃, which is in accordance with the phenomena of less stability observed during the experiment process. After 300 ℃, the framework of as-synthesized SNNU-Bai66 takes place the full collapse. For as-synthesized $Li^+$-SNNU-Bai66 and $DMA^+$-SNNU-Bai66, a few water molecules which may be induced in their pores during the TGA measurement are lost around 60 ℃, and a few of acetone molecules exchanged into the frameworks are lost around 100 ℃. Then, the framework of as-synthesized $Li^+$-SNNU-Bai66 and $DMA^+$-SNNU-Bai66 take place the partial collapse around 200 ℃, and fully collapse after 300 ℃. Notably, the framework of as-synthesized $DMA^+$-SNNU-Bai66 directly collapse around 350 ℃, however, there is a little weight-loss around 350 ℃ in the TG plot of as-synthesized $Li^+$-SNNU-Bai66, which is originated from the loss of crystal water molecules in the $[Li(H_2O)_4]^+$ exchanged in the pores, supported by the literature report in which the crystal water is reported to loss the crystal water molecules only above 300 ℃.[1] Finally, for activated $Li^+$-SNNU-Bai66 and $DMA^+$-SNNU-Bai66, there are a small loss of weight around 60 ℃ in the TGA plot, which may be primarily resulted from the water molecules adsorbed in the pores during the measurement process. Then, their frameworks partially collapses around 200 ℃ and takes place the full collapse after 300 ℃. Similarly, there is also a little weight-loss around 350 ℃ in the TG plot of activated $Li^+$-SNNU-Bai66, which is attributed to the loss of crystal water molecules in the $[Li(H_2O)_4]^+$ exchanged in the pores.[1]

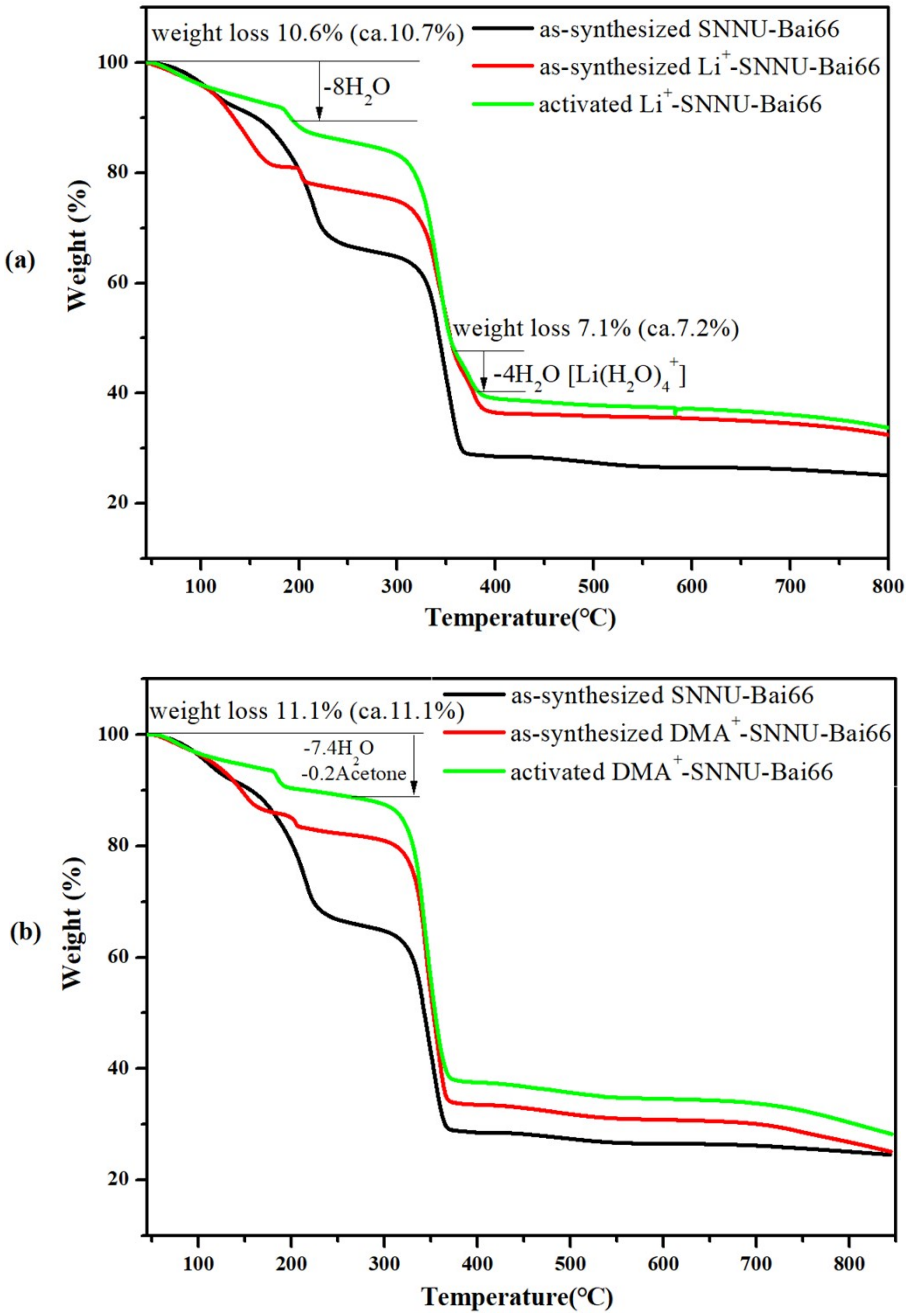


***Figure S8.*** TGA curves of as-synthesized (black), ion-exchange (red) and activated (green) $Li^+$-SNNU-Bai66 (a)/$DMA^+$-SNNU-Bai66 (b).

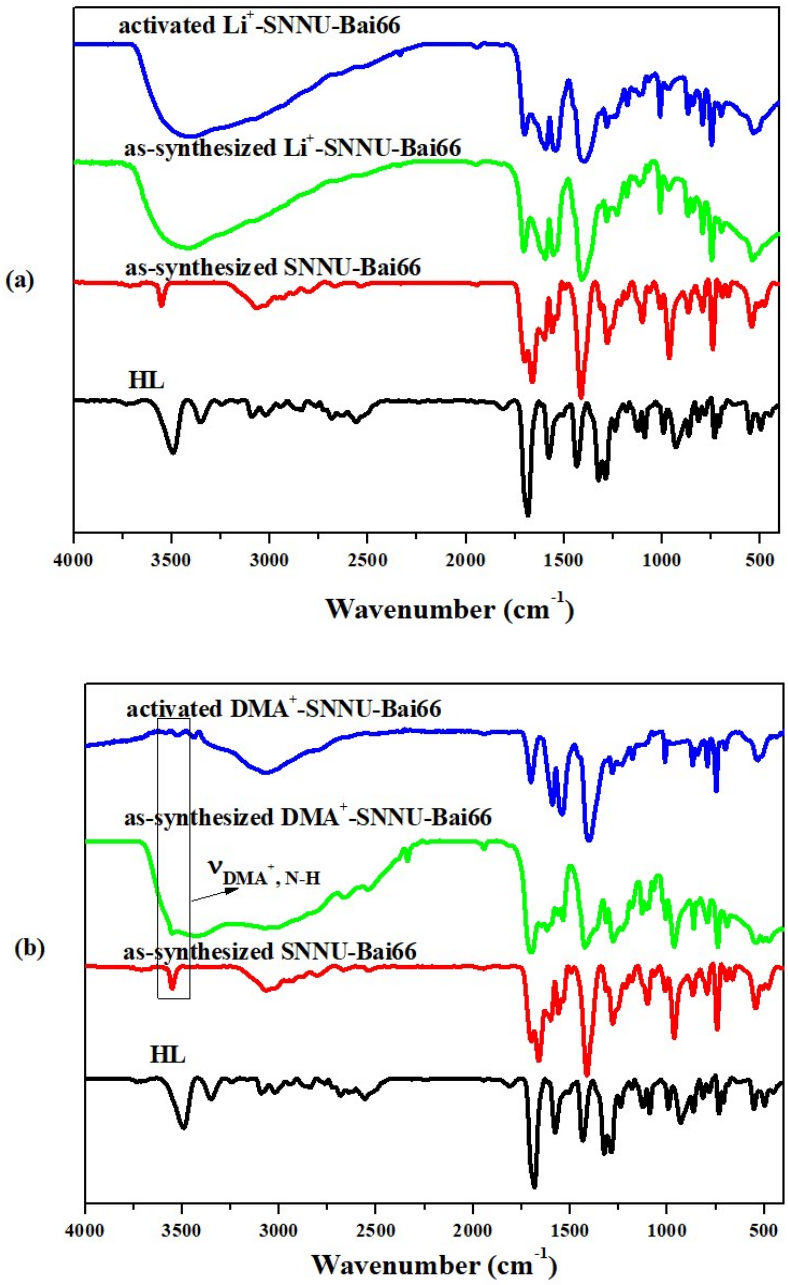


***Figure S9.*** Infrared spectra of ligand, as-synthesized SNNU-Bai66, as-synthesized and activated $Li^+$-SNNU-Bai66 (a)/$DMA^+$-SNNU-Bai66 (b). In the spectrums of as-synthesized SNNU-Bai66, as-synthesized and activated $DMA^+$-SNNU-Bai66, the IR peaks characteristic N-H stretching of $DMA^+$ in the pores are evident at 3551 $cm^{-1}$, 3553 $cm^{-1}$ and 3524 $cm^{-1}$, respectively.[2] However, after the $[Li(H_2O)_4]^+$ exchanged into the pores of as-synthesized and activated $Li^+$-SNNU-Bai66, the IR peaks characteristic N-H stretching of $DMA^+$ in the pores disappeared in the spectrums of as-synthesized and activated $Li^+$-SNNU-Bai66, which indicated the successful ion-exchange in as-synthesized and activated $Li^+$-SNNU-Bai66.

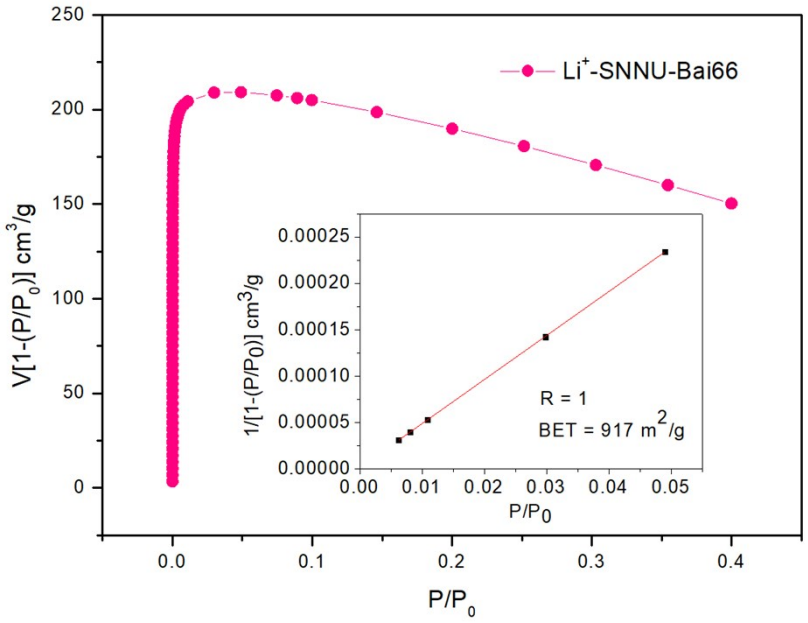


***Figure S10.*** The V[1-(P/$P_0$)] vs. P/$P_0$ for $Li^+$-SNNU-Bai66, only the ranges below P/$P_0$ = 0.05 ($Li^+$-SNNU-Bai66) satisfy the first consistency criterion for applying the BET theory. Inset: Plot of the linear region for the BET equation.

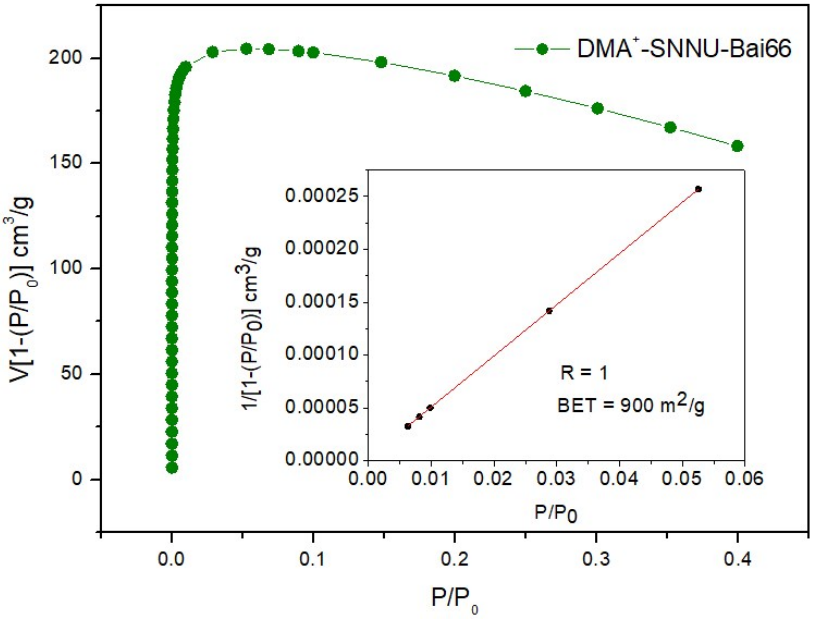


***Figure S11.*** The V[1-(P/$P_0$)] vs. P/$P_0$ for $DMA^+$-SNNU-Bai66, only the ranges below P/$P_0$ = 0.06 ($DMA^+$-SNNU-Bai66) satisfy the first consistency criterion for applying the BET theory. Inset: Plot of the linear region for the BET equation.

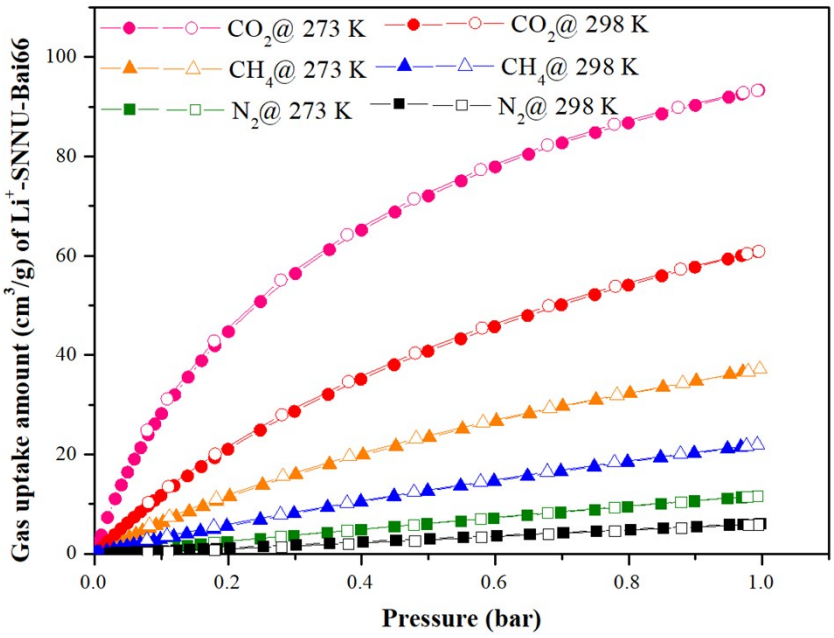


***Figure S12.*** $CO_2$, $N_2$ and $CH_4$ adsorption isotherms for $Li^+$-SNNU-Bai66 at 273 K and 298 K with the unit of gas uptake as $cm^3/g$ (STP); Filled and open symbols represent adsorption and desorption, respectively.

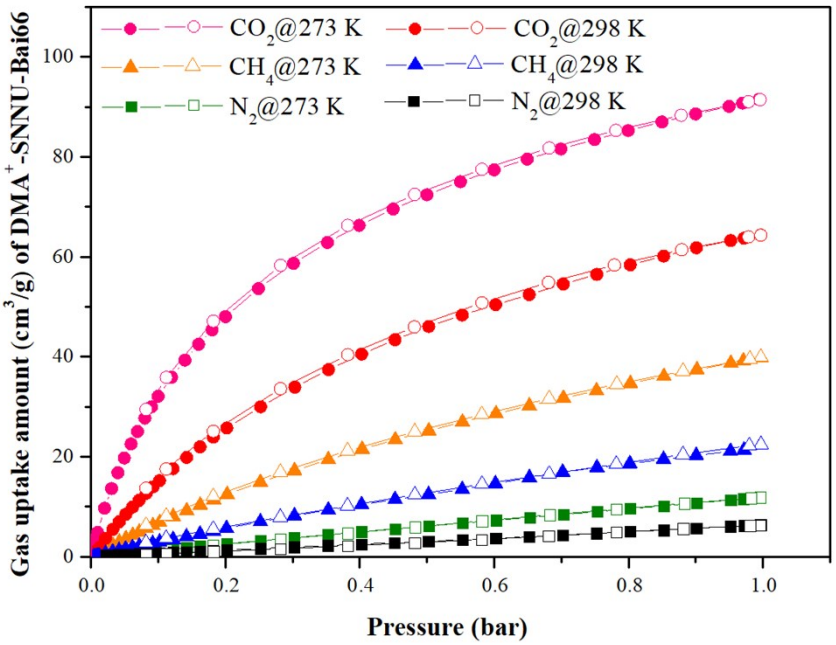


***Figure S13.*** $CO_2$, $N_2$ and $CH_4$ adsorption isotherms for $DMA^+$-SNNU-Bai66 at 273 K and 298 K with the unit of gas uptake as $cm^3/g$ (STP); Filled and open symbols represent adsorption and desorption, respectively.

**Estimation of the isosteric heats of gas adsorption.** A virial-type[3] expression comprising the temperature-independent parameters $a_i$ and $b_j$ was employed to calculate the enthalpies of adsorption for $CO_2$ (at 273 and 298 K) on $Li^+$/$DMA^+$-SNNU-Bai66. In each case, the data were fitted using the equation:

$$\ln P = \ln N + 1/T \sum_{i=0}^{m} a_i N^i + \sum_{j=0}^{n} b_j N^j \qquad (1)$$

Here, $P$ is the pressure expressed in Torr, $N$ is the amount adsorbed in mmol/g, $T$ is thetemperature in K, $a_i$ and $b_j$ are virial coefficients, and $m$, $n$ represent the number of coefficients required to adequately describe the isotherms ($m$ and $n$ were gradually increased until the contribution of extra added $a$ and $b$ coefficients was deemed to be statistically insignificant towards the overall fit, and the average value of the squared deviations from the experimental values was minimized). The values of the virial coefficients $a_0$ through $a_m$ were then used to calculate the isosteric heat of adsorption using the following expression.

$$Q_{st} = -R \sum_{i=0}^{m} a_i N^i \qquad (2)$$

$Q_{st}$ is the coverage-dependent isosteric heat of adsorption and $R$ is the universal gas constant. The heat of $CO_2$ and $CH_4$ sorption for $Li^+$/$DMA^+$-SNNU-Bai66 in the manuscript are determined by using the sorption data measured in the pressure range from 0-1 bar (273 and 298 K), which is fitted by the virial-equation very well ($R^2 > 0.9999$).

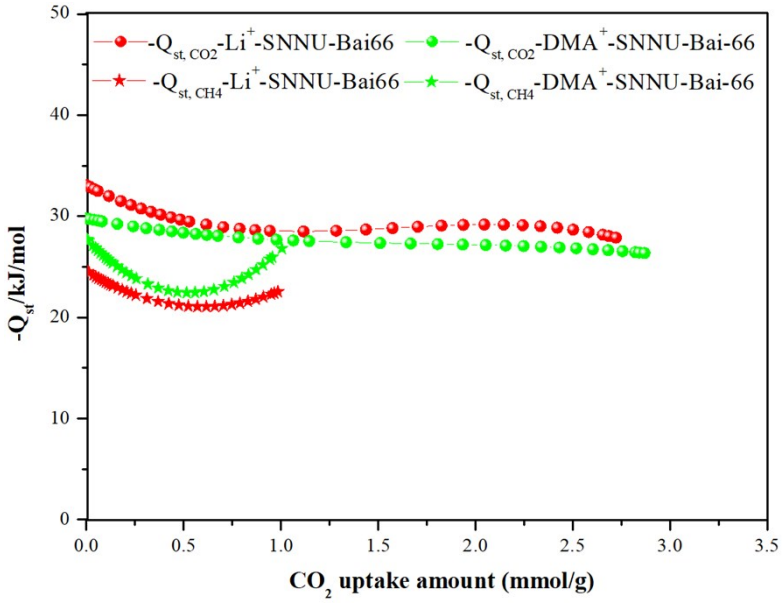


***Figure S14.*** The $CO_2$ (ball) and $CH_4$ (star) adsorption enthalpies of $Li^+$-SNNU-Bai66 (red) and $DMA^+$-SNNU-Bai66 (green).

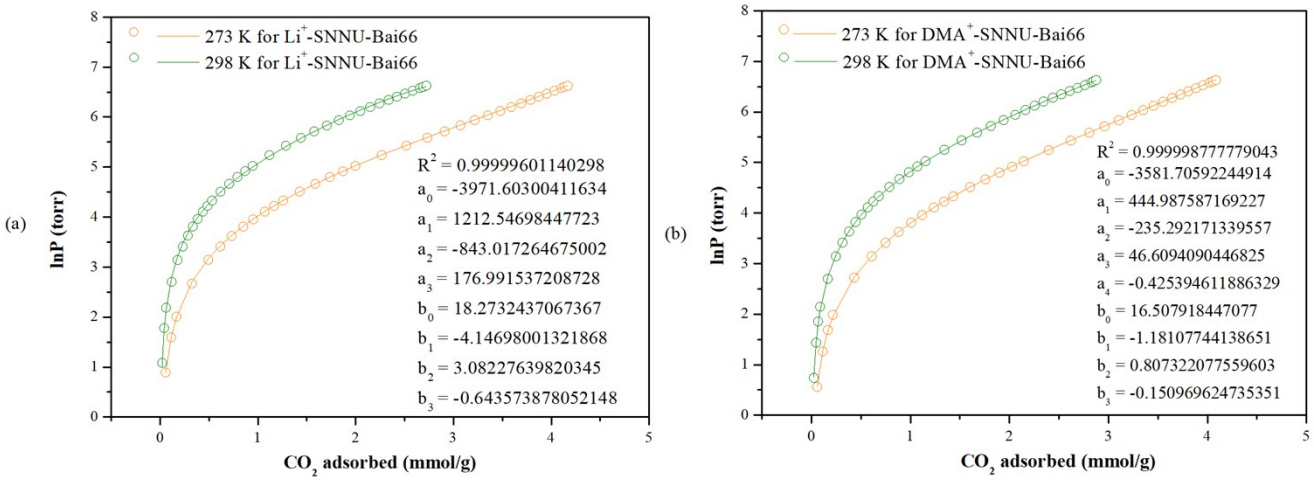


***Figure S15.*** The details of virial equation (solid lines) fitting to the experimental $CO_2$ adsorption data (symbols) for $Li^+$-SNNU-Bai66 (a) and $DMA^+$-SNNU-Bai66 (b).

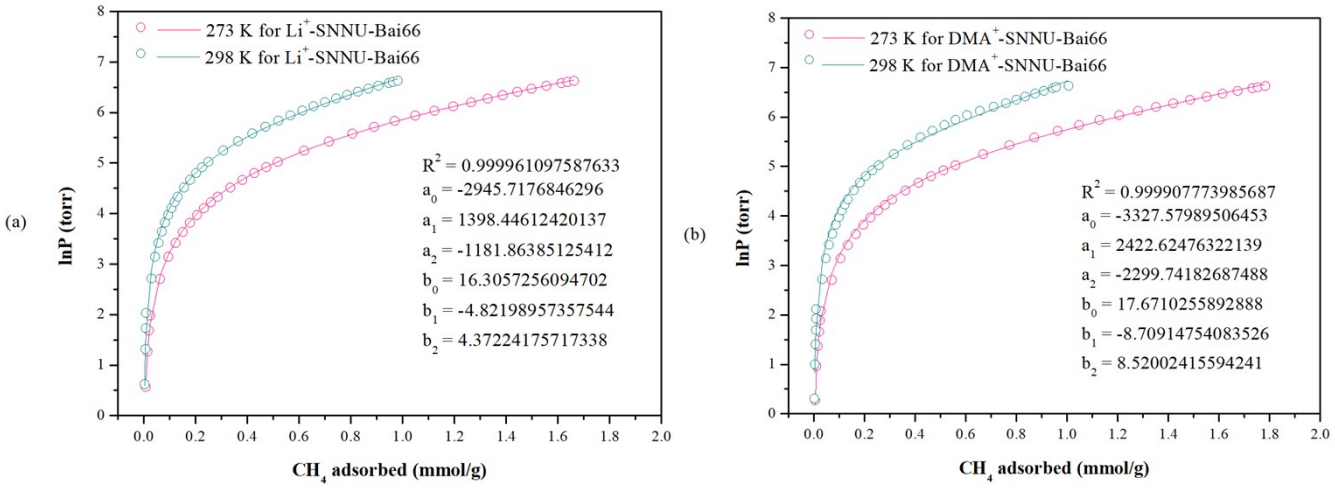


***Figure S16.*** The details of virial equation (solid lines) fitting to the experimental $CH_4$ adsorption data (symbols) for $Li^+$-SNNU-Bai66 (a) and $DMA^+$-SNNU-Bai66 (b).

**Prediction of the Gases Adsorption Selectivity by IAST.** IAST (ideal adsorption solution theory)[4-5] was used to predict binary mixture adsorption from the experimental pure-gas isotherms. In order to perform the integrations required by IAST, the single-component isotherms should be fitted by a proper model. In practice, several methods to do this are available. We found for this set of data that the dual-site Langmuir-Freundlich equation was successful in fitting the data. As can be seen in Figure S18 and Table S2-3, the model fits the isotherms very well ($R^2 > 0.9999$).

$$q = \frac{q_{m,1} b_1 p^{1/n_1}}{1 + b_1 p^{1/n_1}} + \frac{q_{m,2} b_2 p^{1/n_2}}{1 + b_2 p^{1/n_2}} \quad (3)$$

Here, $P$ is the pressure of the bulk gas at equilibrium with the adsorbed phase (kPa), $q$ is the adsorbed amount per mass of adsorbent (mmol/g), $q_{m,1}$ and $q_{m,2}$ are the saturation capacities of sites 1 and 2 (mmol/g), $b_1$ and $b_2$ are the affinity coefficients of sites 1 and 2 (1/kPa), and $n_1$ and $n_2$ represent the deviations from an ideal homogeneous surface. The fitted parameters were then used to predict multi-component adsorption with IAST.

The selectivity $S_{A/B}$ in a binary mixture of components A and B is defined as $(x_A/y_A)/(x_B/y_B)$, where $x_i$ and $y_i$ are the mole fractions of component $i$ ($i$ = A , B) in the adsorbed and bulk phases, respectively.

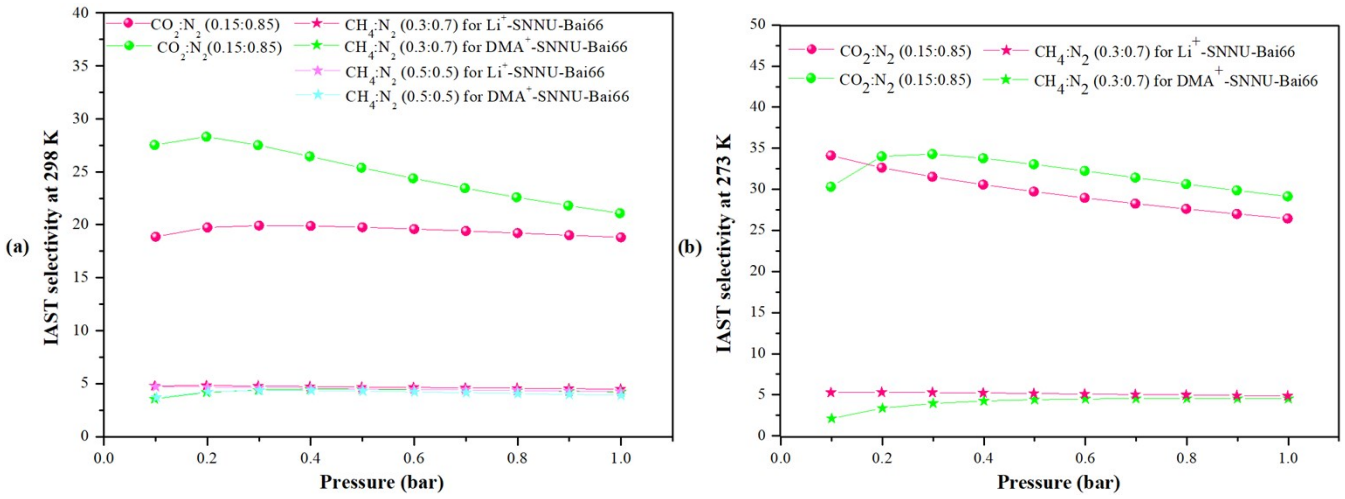


***Figure S17.*** IAST predicted selectivity for $CO_2/N_2$ (0.15:0.85) and $CH_4/N_2$ (0.3:0.7 and 0.5:0.5) mixture of $Li^+$-SNNU-Bai66 and $DMA^+$-SNNU-Bai66 at 298 K (a) and 273 K (b).

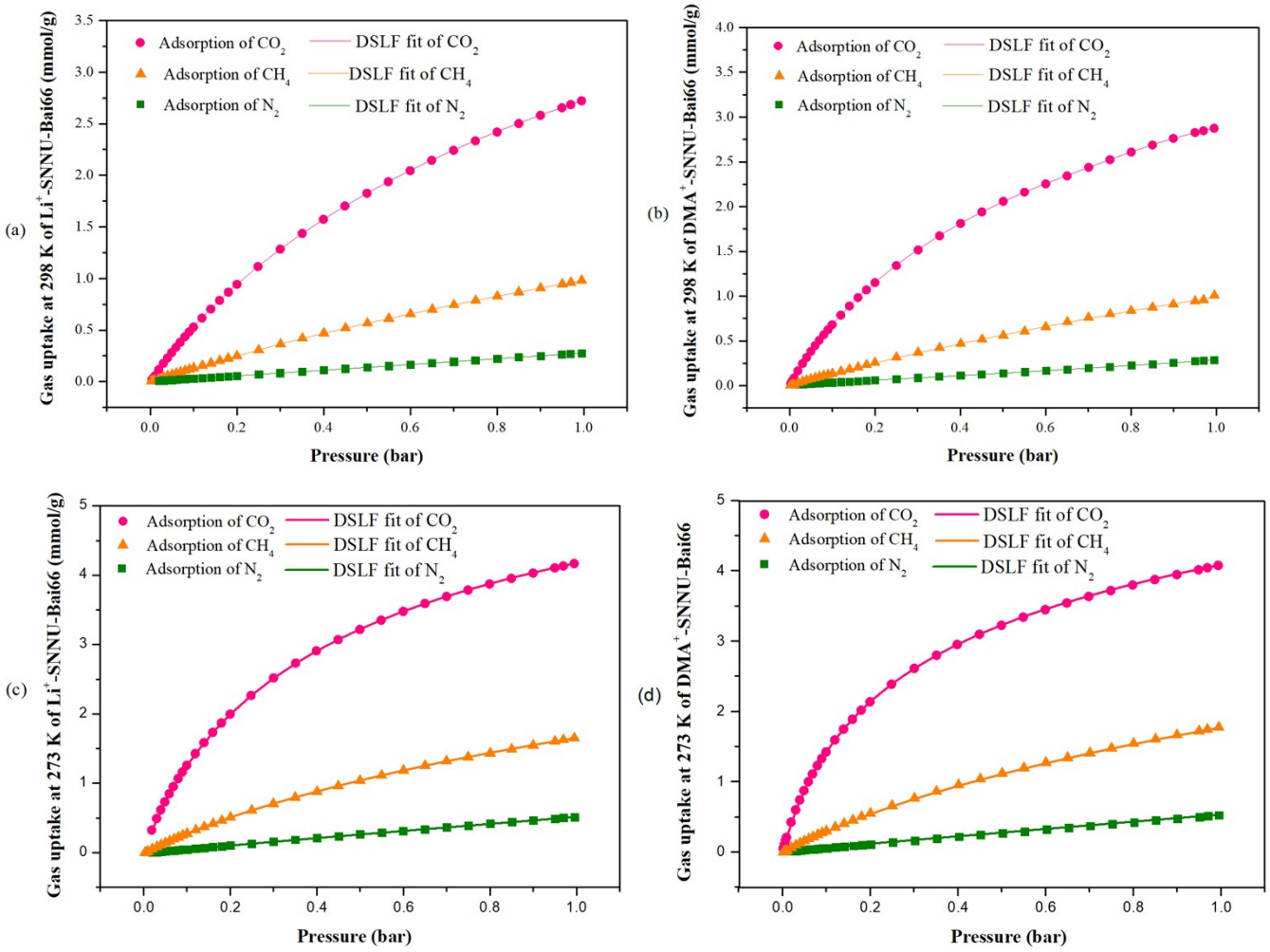


***Figure S18.*** Low pressure gas adsorption isotherms and the dual-site Langmuir-Freundlich (DSLF) fit lines of $CO_2$, $N_2$ and $CH_4$ in $Li^+$-SNNU-Bai66 (a, c) and $DMA^+$-SNNU-Bai66 (b, d) at 298 K and 273 K, respectively.

***Table S2.*** Dual-site Langmuir-Freundlich parameters for pure $CO_2$, $N_2$ and $CH_4$ isotherms in $Li^+$-SNNU-Bai66 at 298 K and 273 K

| T | | $Li^+$-SNNU-Bai66 | | |
|---|---|---|---|---|
| | | $CO_2$ | $N_2$ | $CH_4$ |
| 298 K | $R^2$ | 0.99999458023487 | 0.999984479449835 | 0.999978847496215 |
| | $q_{m,1}$ | 0.561061741419909 | 52.5527087878162 | 5.22578283066881 |
| | $q_{m,2}$ | 5.09419173390377 | 0.00411464501357894 | 0.0127430159337264 |
| | $b_1$ | 0.0446820097982997 | 0.0000459357882704641 | 0.00288978079205831 |
| | $b_2$ | 0.00647286343358193 | 0.0269439973967706 | 9.57809871345727E-11 |
| | $n_1$ | 0.943636333 | 0.972170082 | 1.054104207 |
| | $n_2$ | 0.958803242 | 0.097683298 | 0.141613473 |
| 273 K | $R^2$ | 0.999998692000102 | 0.999983359391146 | 0.999983504074874 |
| | $q_{m,1}$ | 3.21908891057571 | 791.307785779455 | 0.306374058687683 |
| | $q_{m,2}$ | 3.29127198897272 | 0.00394648204238499 | 4.22758356992263 |
| | $b_1$ | 0.0448547767253429 | 7.96024019244476E-06 | 0.0408035667961173 |
| | $b_2$ | 0.0144339053171336 | 2.01210578135025E-10 | 0.00448345657119935 |
| | $n_1$ | 1.070694 | 1.04224 | 0.969356 |
| | $n_2$ | 1.069863 | 0.136329 | 0.976328 |

***Table S3.*** Dual-site Langmuir-Freundlich parameters for pure $CO_2$, $N_2$ and $CH_4$ isotherms in $DMA^+$-SNNU-Bai66 at 298 K and 273 K

| T | | $DMA^+$-SNNU-Bai66 | | |
|---|---|---|---|---|
| | | $CO_2$ | $N_2$ | $CH_4$ |
| 298 K | $R^2$ | 0.999986925094979 | 0.999859477493165 | 0.999736748010251 |
| | $q_{m,1}$ | 0.0597858891562868 | 2608.54364092917 | 0.00917708606156013 |
| | $q_{m,2}$ | 4.78630605552981 | 35.319892279208 | 4.17410719902989 |
| | $b_1$ | 2.49862056898043E-31 | 5.20580133579653E-08 | 5.49504672126615E-06 |
| | $b_2$ | 0.0190010389445305 | 0.000191046764809464 | 0.00311417669799898 |
| | $n_1$ | 0.062105376 | 0.655185767 | 0.052645884 |
| | $n_2$ | 1.06428987 | 1.539056004 | 1.003036008 |
| 273 K | $R^2$ | 0.999993317301959 | 0.99998028520507 | 0.999986871258461 |
| | $q_{m,1}$ | 3.71167459203402 | 3559.32724641671 | 0.737671661005768 |
| | $q_{m,2}$ | 3.46960071158527 | 3.14150142005496 | 4.90225387086551 |
| | $b_1$ | 0.00682322385628771 | 1.64316107432735E-06 | 0.0281645031369217 |
| | $b_2$ | 0.0641624663056007 | 0.00233370332437391 | 0.00282751361770271 |
| | $n_1$ | 1.075874 | 1.024425 | 1.001817 |
| | $n_2$ | 1.072205 | 14.57625 | 0.96136 |

***Table S4.*** Comparison of greenhouse gas capture properties of $Li^+$-SNNU-Bai66 and $DMA^+$-SNNU-Bai66 with those of some well-known porous solid materials with functionalized pore surface at 298 K

| MOF | $CO_2$ uptake/ $cm^3/g$ | | $CH_4$ uptake/ $cm^3/g$ | | $N_2$ uptake 1.0 bar, $cm^3/g$ | $-Q_{st}$ ($CO_2$) kJ/mol | $-Q_{st}$ ($CH_4$) kJ/mol | $S_{IAST, 298\ K}$ | |
|---|---|---|---|---|---|---|---|---|---|
| | 0.15 bar | 1.0 bar | 0.3 bar | 1.0 bar | | | | $CO_2$:$N_2$/0.15:0.85 | $CH_4$:$N_2$/0.3:0.7 |
| SIFSIX-2-Cu[6] | 8.1 | 130 | - | - | 3.6 | 22 | - | 13.7(0.1:0.9) | - |
| PCN-61[7] | 12.5 | 100.8 | - | - | 4.3 | 22 | - | 15(0.5:0.5) | - |
| NJU-Bai0[7] | 21.3 | 114.2 | - | - | 5.4 | 26.3 | - | 22(0.5:0.5) | - |
| Bio-MOF-11[8] | 35.0 | 105 | - | - | 7.0 | 33.1 | - | 43(0.1:0.9) | - |
| **$Li^+$-SNNU-Bai66** | **16.7** | **61.0** | **8.1** | **22.0** | **6.2** | **33.0** | **24.5** | **18.8** | **4.5** |
| **$DMA^+$-SNNU-Bai66** | **21.0** | **64.4** | **8.3** | **22.5** | **6.4** | **29.8** | **27.7** | **21.1** | **4.1** |
| Zeolite-5A[9] | - | - | 6.7 | 20.8 | - | - | 9.9[10] | - | 0.9(0.5:0.5) |
| HKUST-1[9] | - | - | 7.8 | 20.2 | - | - | 17.0 | - | 3.7(0.5:0.5) |
| MOF-74-Ni[9,11] | - | - | 23.0[11] | 42.8 | 20.0[11] | - | 20.6 | - | 3.8(0.5:0.5) |
| ATC-Cu[9] | - | - | 33.6 | 65.0 | 16.8 | - | 26.8 | - | 9.7(0.5:0.5) |
| | | | | | | | | | 8.8(0.3:0.7) |

***Table S5.*** Selective greenhouse gas adsorption properties and functional adsorption sites of some representative ionic MOFs at 298 K

| Ionic MOF | Gas uptake/ $cm^3/g$ | | $S_{IAST}$ | | Functional site |
|---|---|---|---|---|---|
| | $CO_2$, 0.15 bar | $CH_4$, 1.0 bar | $CO_2:N_2$/0.15:0.85 | $CH_4:N_2$/0.5:0.5 | |
| Y-FTZB-MOF[12] | 30.2 | - | 16[a] | - | ES[b]+ N donor+OMS+F |
| Fe-BTT[13] | 28.0 | - | 5.5[c] | - | ES + N donor+OMS |
| NJU-Bai27[14] | 25.5 | 26.9 | 217 | - | ES + OMS |
| SNU-100'-Co[1b] | 25.0 | - | 31.0 (27.0)[d] | - | ES |
| CPF-13[15] | 24.6 | - | 9.5[e] | - | ES + $NH_2$ |
| NJU-Bai49[16] | 22.9 | 20.1 | 166.7 | - | ES + amide |
| $[Mn_2(Hcbptz)_2(Cl)(H_2O)]Cl$[17] | 22.2 | 15.0 | 78.3 | - | ES +N donor+OMS+Cl |
| **$DMA^+$-SNNU-Bai66** | **21.0** | **22.5** | **21.1** | **4.1(0.3:0.7)** | **ES +N donor +Cl** |
| SNNU-61[16] | 20.4 | - | - | - | ES |
| NJU-Bai51[18] | 20.2 | 17.9 | 545.7 | - | ES + OMS |
| NJU-Bai25[14] | 17.8 | 22.4 | 99 | - | ES + OMS |
| **$Li^+$-SNNU-Bai66** | **16.7** | **22.0** | **18.8** | **4.5(0.3:0.7)** | **ES +N donor +Cl** |
| LCU-102[19] | 12.5 | - | 60 (273 K) | | ES + OMS |
| SNU-151'[20] | 12.5 | 20.0 | 30 | - | ES + OMS |
| ZJNU-55[21] | 12.0 | 8.5 | - | - | ES + N donor+COOH |
| TEA-Bio-MOF-1[22] | 11.9 | - | - | - | ES + N donor |
| NJU-Bai34[2] | 11.5 | 11.2 | 60.1 | - | ES + COOH |
| NJU-Bai50[18] | 11.0 | 16.8 | 30.5 | - | ES + OMS |
| TMU-5[23] | 8.0 | - | - | - | ES + N donor |

*Note:* when the data is not able to be found in the work, it is estimated from the adsorption isotherm or IAST plot in the work; *a*. $S_{IAST,\ CO_2:N_2/0.1:0.9}$; *b.* electrostatic sites, denoted as ES; *c.* $q_{CO2,\ 0.15\ bar}/q_{N2,\ 0.75\ bar}$; *d*. Selectivity was calculated from the ratios of Henry constants for $CO_2$ and $N_2$ adsorption isotherms at 298 K and the values in parenthesis is selectivity estimated by using the molar ratio at 298 K of the $CO_2$ uptake at 0.15 atm and the $N_2$ uptake at 0.85 atm; *e.* Selectivity was calculated from the ratios of Henry constants for $CO_2$ and $N_2$ adsorption isotherms at 298 K.

***Table S6.*** Selective $CH_4$ adsorption properties and functional adsorption sites of some representative MOFs at 298 K

| MOF | $CH_4$ uptake/ $cm^3/g$ | | $S_{IAST}$ | Functional site |
|---|---|---|---|---|
| | 0.3 bar | 1.0 bar | $CH_4$:$N_2$/0.5:0.5 | |
| ATC-Cu[9] | 33.6 | 65.0 | 9.7 | OMS |
| MOF-74-Ni[9,11] | 23.0[11] | 42.8 | 3.8 | OMS |
| Ni-MOF[24] | 17.9 | 42.6 | 7.0 | N donor |
| **$DMA^+$-SNNU-Bai66** | **8.3** | **22.5** | **4.1(0.3:0.7)** | **ES[a] + Cl** |
| **$Li^+$-SNNU-Bai66** | **8.1** | **22.0** | **4.5(0.3:0.7)** | **ES + Cl** |
| HKUST-1[9] | 7.84 | 20.2 | 3.7 | OMS |
| Zeolite-5A[9] | 6.72 | 20.8 | 0.9 | Polar pore surface |
| $Cu(INA)_2$[25] | 6.0 | 18.6 | 6.9*b* | $O_{COO^-}$ |
| $Ni_2(HCOO)_6$[25] | 6.7 | 17.7 | 6.2*b* | - |
| Cu-MOF[26] | 4.9 | 10.5 | 6.9*c* | $CF_3$ |
| $Co_3(C_4O_4)(OH)_2$[27] | 6.6 | 9.05 | 12.5 | $OH^-$ |

*Note:* when the data is not able to be found in the work, it is estimated from the adsorption isotherm or IAST plot in the work; *a*. electrostatic sites, denoted as ES; *b.* $\alpha_{CH4/N2} = \kappa_{CH4}/\kappa_{N2}$; *c.* $S = \Delta q_i/\Delta q_j * \alpha_{ij}$.

**Computation Detail.** Atomistic GCMC simulations were performed to estimate the adsorption isotherms of $CO_2$ and $CH_4$ in $Li^+$-SNNU-Bai66 and $DMA^+$-SNNU-Bai66. All simulations/calculations were performed by the Materials Studio 7.0 package. DFT and PDFT calculations were performed by the Dmol3 module, using the generalized gradient approximation (GGA) with the Perdew-Burke-Ernzerhof (PBE) functional and the double numerical plus d-functions (DNP) basis set, TS for DFT-D correction, and the Effective Core Potentials (ECP). [28,29]

**MOF models.** The framework of $DMA^+$-SNNU-Bai66 was fixed from the crystallographic data of SNNU-Bai66. For $Li^+$-SNNU-Bai66, the charge of the anionic framework of SNNU-Bai66 has to be balanced by the counterion of $[Li(H_2O)_4]^+$. The preferred adsorption locations of $[Li(H_2O)_4]^+$ cation were searched through Grand Canonical Monte Carlo (GCMC) simulations by using the location task and metropolis method in the sorption calculation module.[29] The framework and $[Li(H_2O)_4]^+$ cation were described by the universal force field (UFF). Both the framework and $[Li(H_2O)_4]^+$ cation were regarded as rigid. The ESP charges estimated from those of cages and clusters in anionic SNNU-Bai66 through DFT performed by the Dmol3 module were assigned to the atoms of the anionic framework and $[Li(H_2O)_4]^+$ cation. The cutoff distance was set to 18.5 Å for the Lennard-Jones (LJ) interactions, and the electrostatic interactions and the van der Waals interactions were handled using the Ewald and Atom based summation method, respectively. The loading steps, production steps and temperature cycles were set to $1 \times 10^5$, $1 \times 10^7$ and 40, respectively.

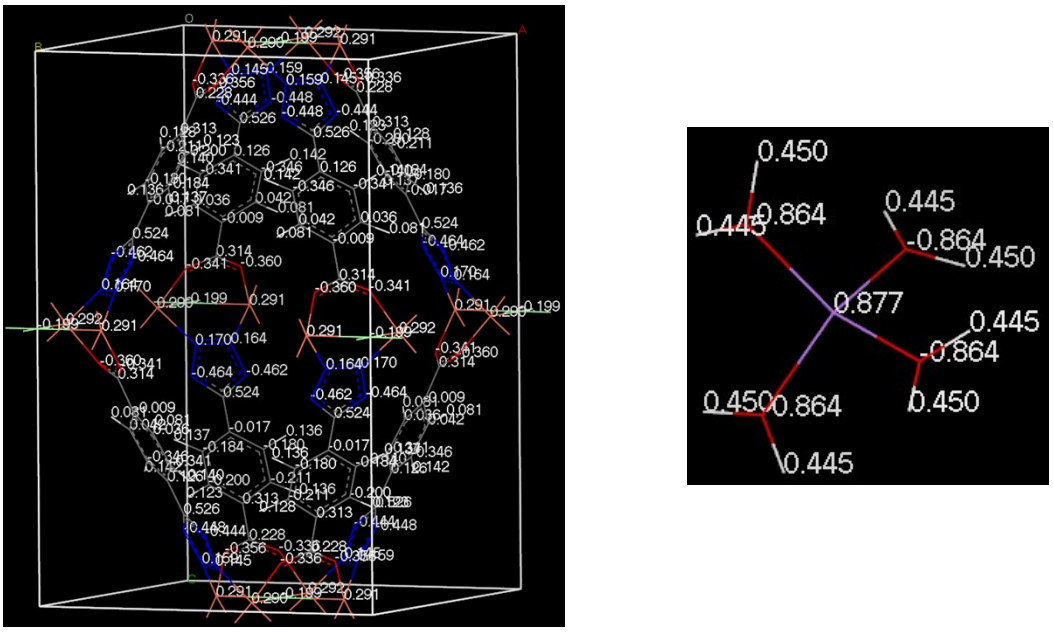


***Figure S19.*** The estimated ESP charges for the atoms of the anionic framework (left) and $[Li(H_2O)_4]^+$ cation (right) during the model of $Li^+$-SNNU-Bai66.

**Gas molecule models.** The $CO_2$ gas molecules were modeled according to the literature reported by Garikoitz Beobide's group[30], and the $CH_4$ gas molecule was modeled according to the report of Omar K. Farha's group [31].

**Binding energy calculation.** The binding energies between the frameworks and $CO_2$ or $CH_4$ gas molecules at special adsorption sites were calculated through PDFT simulations by using the energy task in the Dmol3 module. According to the literature reported by Jiepeng Zhang's group[29], the binding energy is expressed as

$$E_{binding} = E_{host+guest} - E_{host} - E_{guest} \quad (4)$$

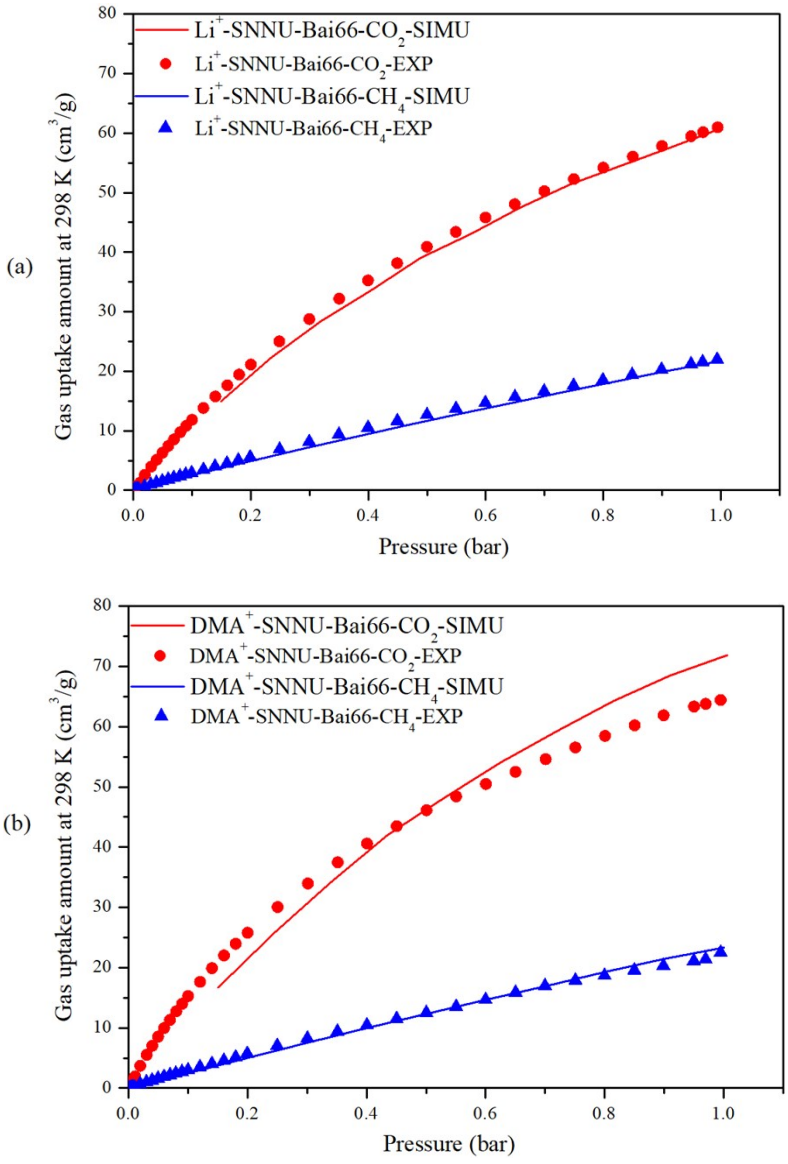


***Figure S20.*** Low pressure gas adsorption isotherms (symbol for experimental data, line for GCMC simulation data) of $CO_2$ (red) and $CH_4$ (blue) in $Li^+$-SNNU-Bai66 (a) and $DMA^+$-SNNU-Bai66 (b) at 298 K.

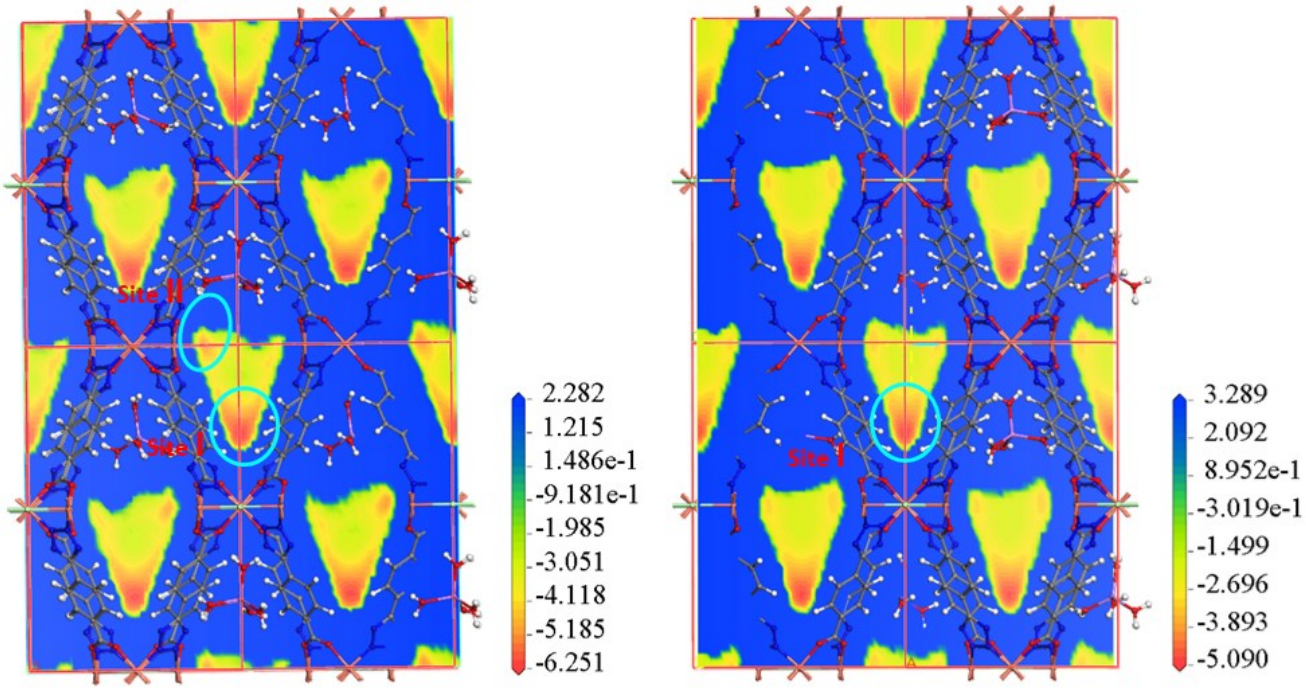


***Figure S21.*** Slice through the calculated potential field for $CO_2$ (left) and $CH_4$ (right) in $Li^+$-SNNU-Bai66 at 298 K and 1 bar simulated by GCMC.

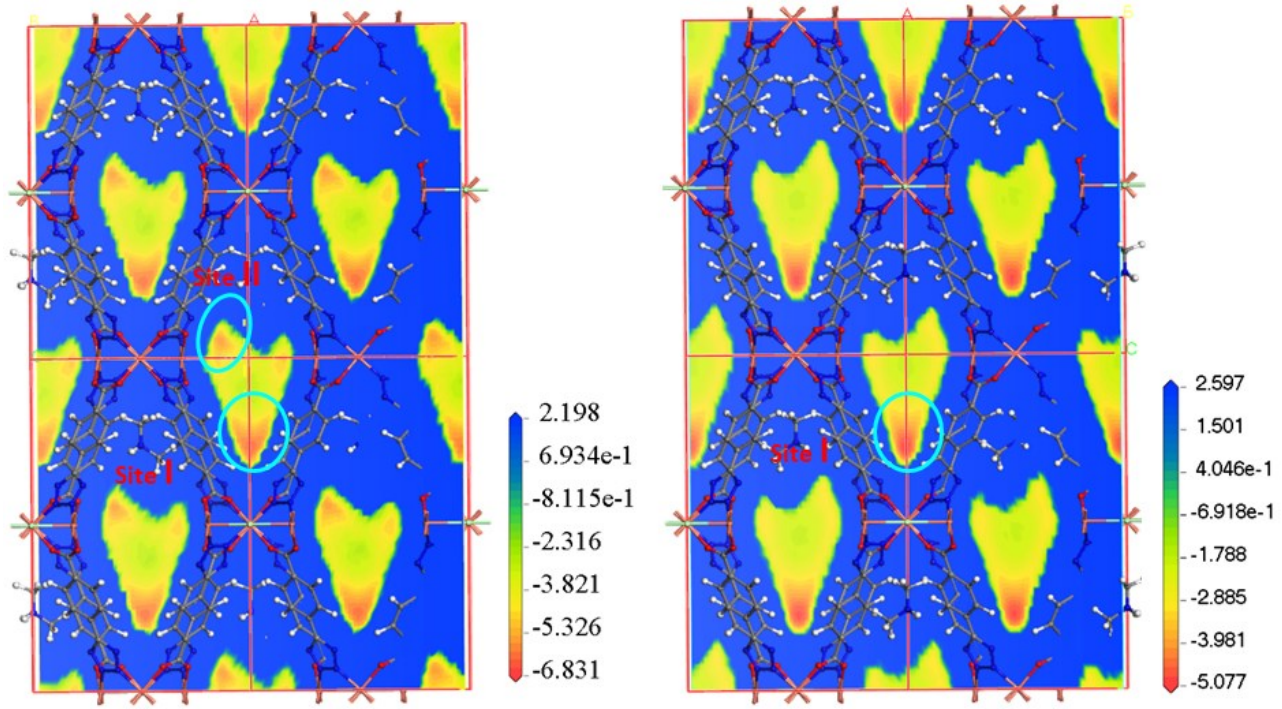


***Figure S22.*** Slice through the calculated potential field for $CO_2$ (left) and $CH_4$ (right) in $DMA^+$-SNNU-Bai66 at 298 K and 1 bar simulated by GCMC.

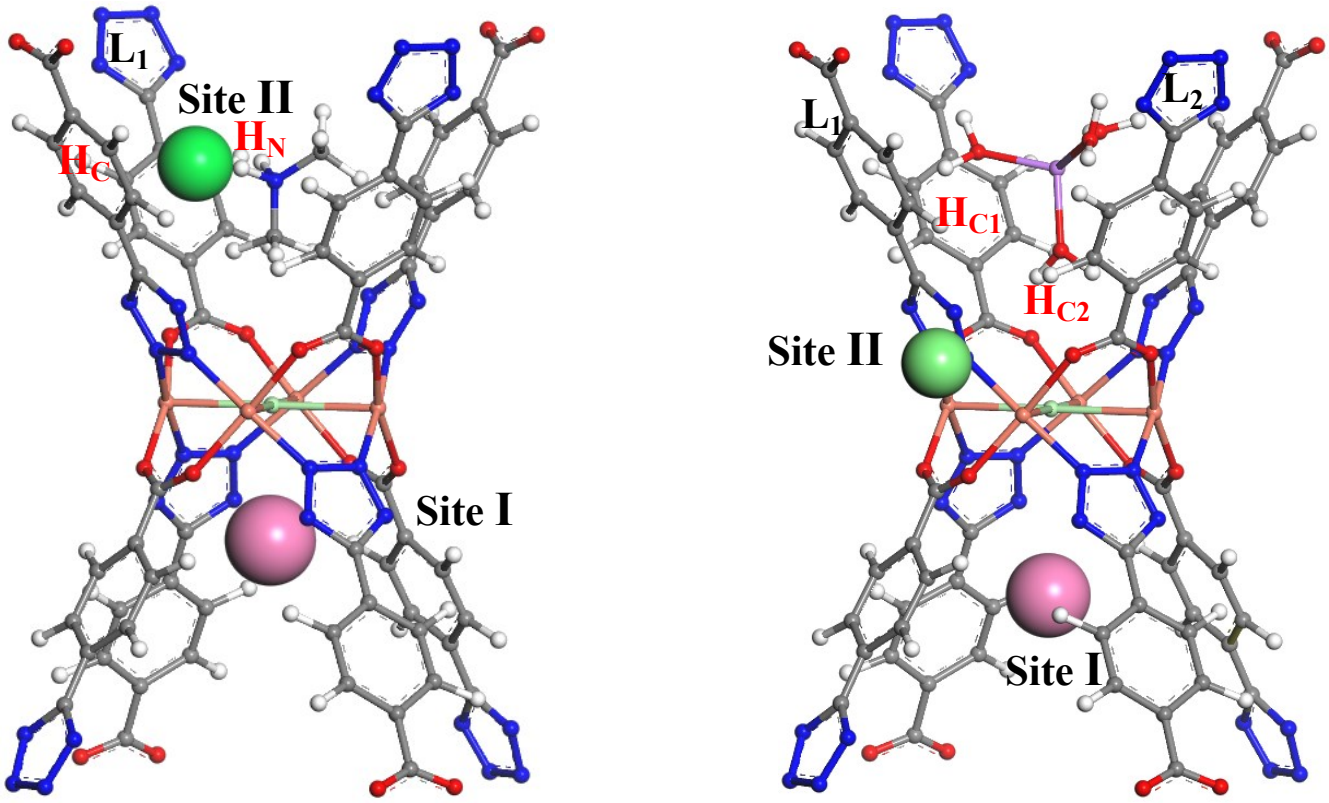


***Figure S23.*** Two primary possible adsorption sites with site I for $CO_2$ and $CH_4$ gas molecules and site II for $CO_2$ gas molecule in $DMA^+$-SNNU-Bai66 (left, with site I being located at the opposite side of $Cl^-$ toward $DMA^+$ and site II being located at the position between the $H_c$ atom of $L_1$ ligand and $DMA^+$) and $Li^+$-SNNU-Bai66 (right, with site I being located at the opposite side of $Cl^-$ toward $Li(H_2O)_4^+$ and site II being located at the position outside the $L_1$ and the $L_2$ ligand near both the $H_{c1}$ atom and $H_{c2}$ atom).

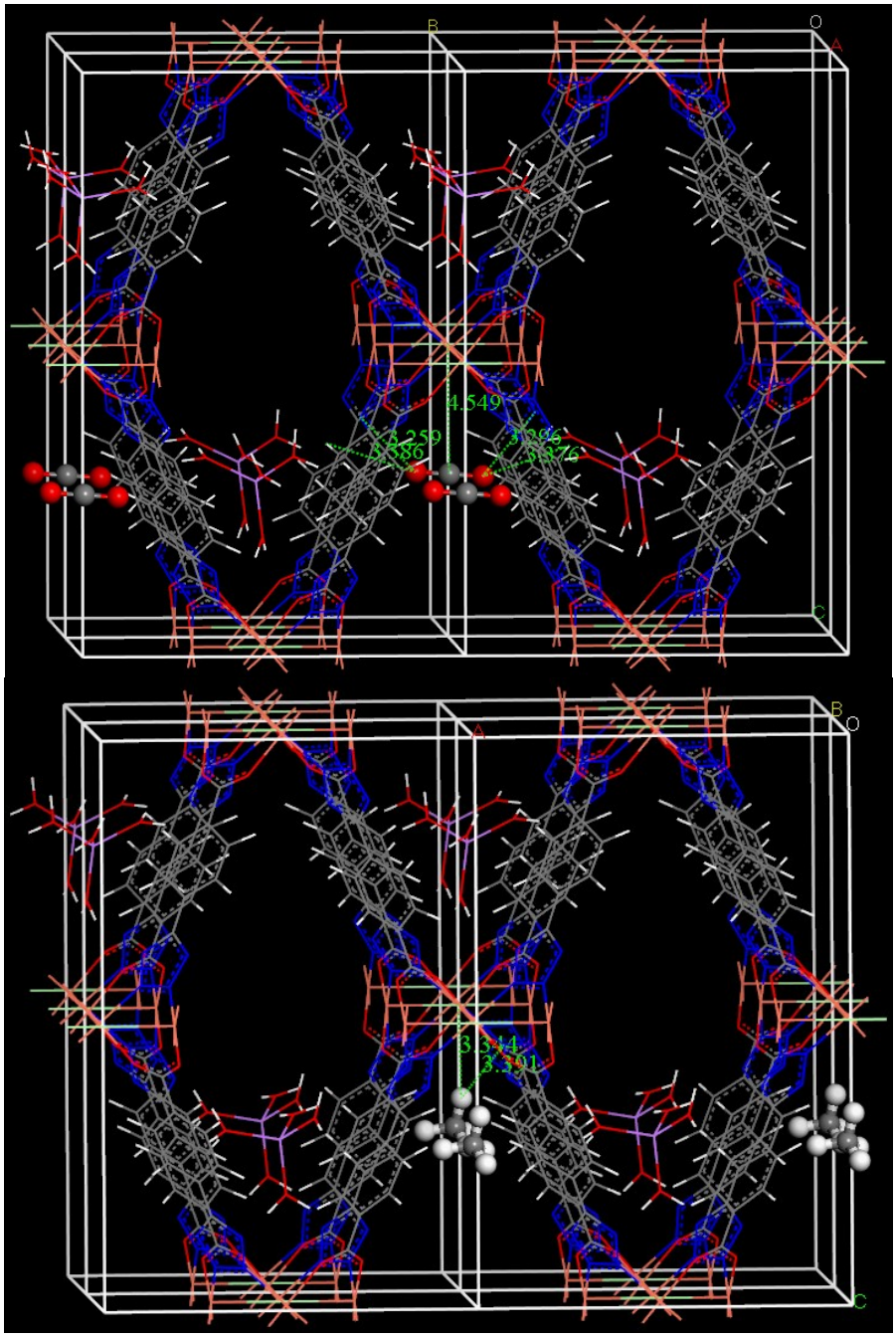


***Figure S24.*** The preferred adsorption site (site I) for $CO_2$ (up) and $CH_4$ (down) in $Li^+$-SNNU-Bai66 simulated by GCMC.

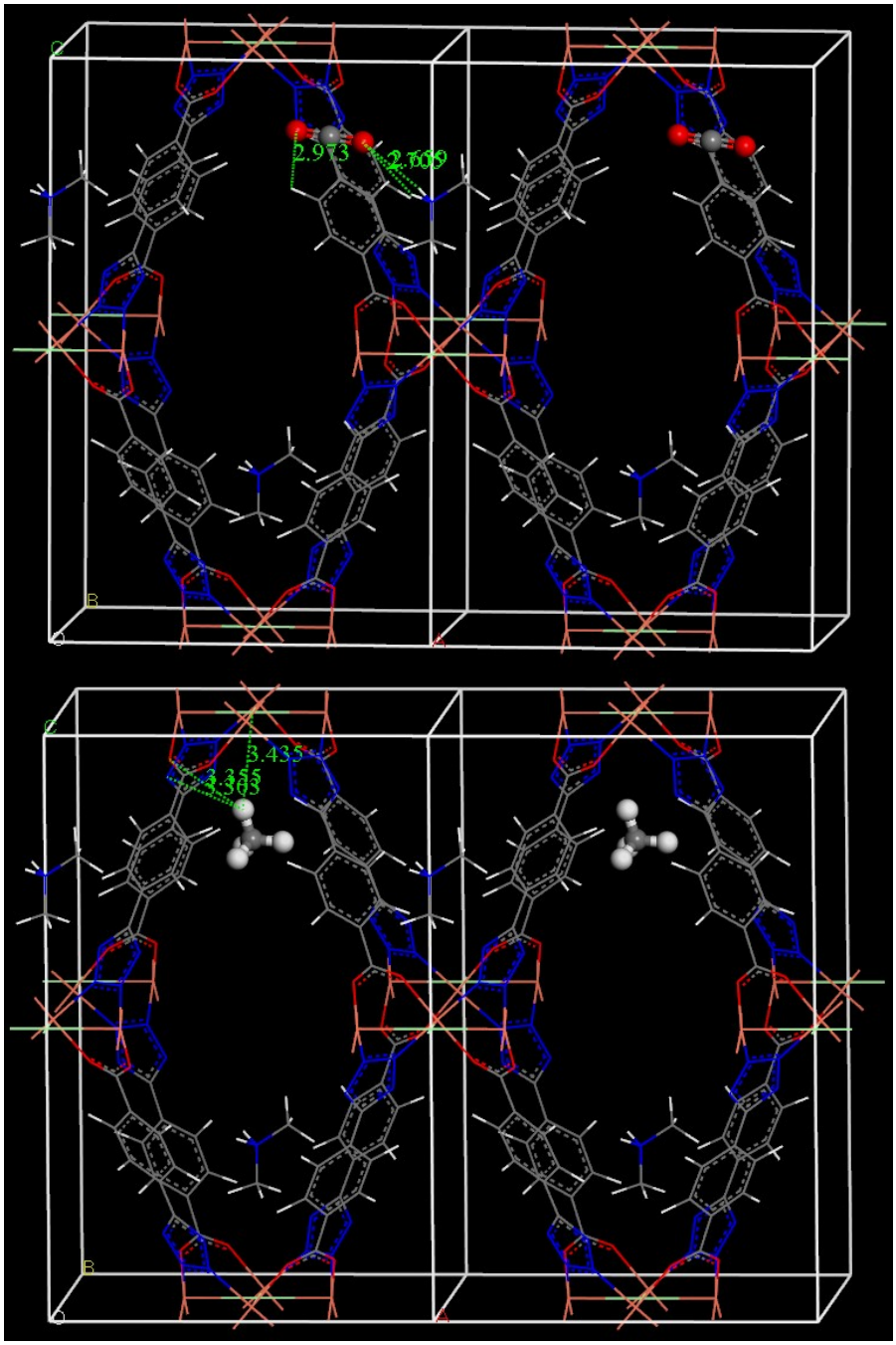


***Figure S25.*** The preferred adsorption site (site II) for $CO_2$ (up) and the preferred adsorption site (site I) for $CH_4$ (down) in $DMA^+$-SNNU-Bai66 simulated by GCMC.

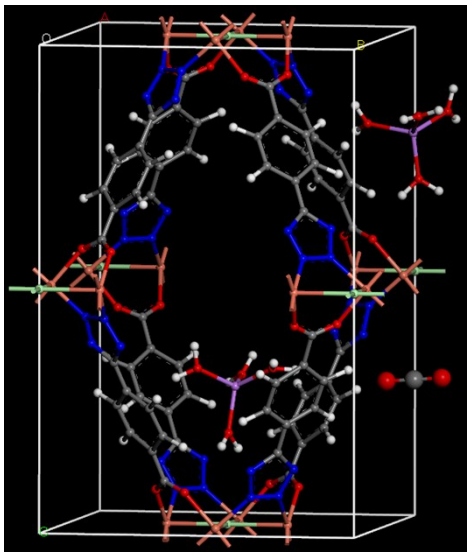

$E_{binding,\ CO2}$ = -33.5 kJ/mol

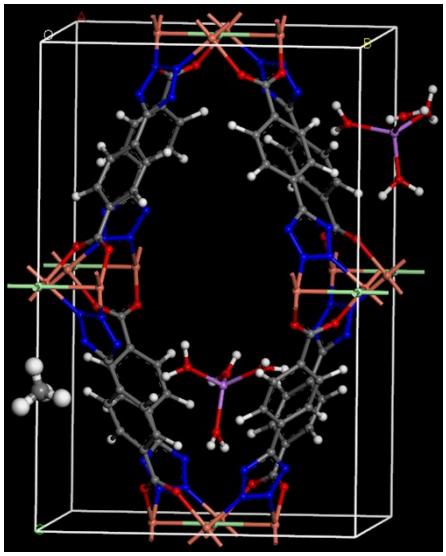

$E_{binding,\ CH4}$ = -40.7 kJ/mol

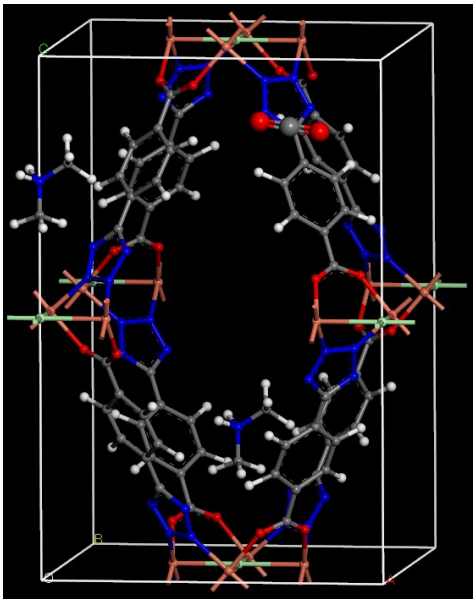

$E_{binding,\ CO2}$ = -42.4 kJ/mol

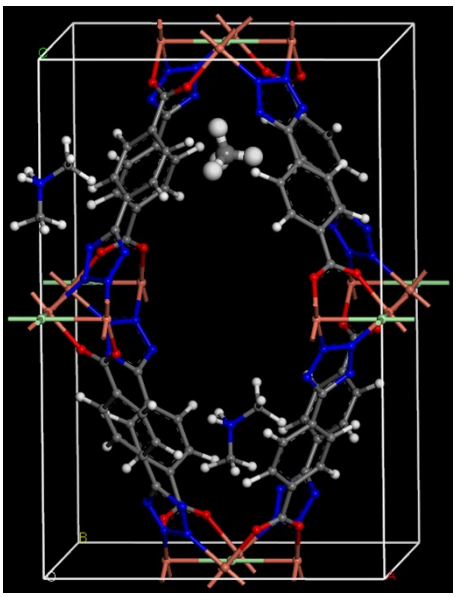

$E_{binding,\ CH4}$ = -38.8 kJ/mol

***Figure S26.*** The binding energy calculated for $Li^+$-SNNU-Bai66 (up) and $DMA^+$-SNNU-Bai66 (down) with one $CO_2$ (left) or $CH_4$ (right) molecule adsorbed in one unit cell.

# Reference


[1] a) F. Nouar, J. Eckert, J. F. Eubank, P. Forster and M. Eddaoudi, *J. Am. Chem. Soc.*, 2009, **131**, 2864-2870； b) H. J. Park and M. P. Suh, *Chem. Sci.*, 2013, **4**, 685-690; c) S. Yang, X. Lin, A. J. Blake, G. S. Walker, P. Hubberstey, N. R. Champness and M. Schröder, *Nat. Chem.*, 2009, **1**, 487-493.

[2] J. Jiang, Z. Lu, M. Zhang, J. Duan, W. Zhang, Y. Pan and J. Bai, *J. Am. Chem. Soc.*, 2018, **140**, 17825-17829.

[3] J. L. C. Rowsell, O. M. Yaghi, *J*. *Am*. *Chem*. *Soc*. **2006**, *128*, 1304.

[4] A. L. Myers, J. M. Prausnitz, *AIChE J.* **1965**, *11*, 121.

[5] a) Y. S. Bae, K. L. Mulfort, H. Frost, P. Ryan, S. Punnathanam, L. J. Broadbelt, J. T. Hupp, R. Q. Snurr, *Langmuir* **2008**, *24*, 8592; b) B. Mu, F. Li, K. S. Walton, *Chem. Commun.* **2009**, 2493.

[6] P. Nugent, Y. Belmabkhout, S. D. Burd, A. J. Cairns, R. Luebke, K. Forrest, T. Pham, S. Ma, B. Space, L. Wojtas, M. Eddaoudi and M. J. Zaworotko, *Nature*, 2013, **495**, 80-84.

[7] B. Zheng, J. Bai, J. Duan, L. Wojtas and M. J. Zaworotko, *J*. *Am*. *Chem*. *Soc*., 2011, **133**, 748-751.

[8] T. Li, D.-L. Chen, J. E. Sullivan, M. T. Kozlowski, J. K. Johnson and N. L. Rosi, *Chem. Sci.*, 2013, **4**, 1746-1755.

[9] Z. Niu, X. Cui, T. Pham, P. C. Lan, H. Xing, K. A. Forrest, L. Wojtas, B. Space and S. Ma, *Angew. Chem. Int. Ed.*, 2019, **58**, 10138-10141.

[10] G.-M. Nam, B.-M. Jeong, S.-H. Kang, B.-K. Lee and D.-K. Choi, *J. Chem. Eng. Data*, 2005, **50**, 72-76.

[11] L. Li, J. Yang, J. Li, Y. Chen and J. Li, *Micropor. Mesopor. Mat.*, 2014, **198**, 236-246.

[12] D.-X. Xue, A. J. Cairns, Y. Belmabkhout, L. Wojtas, Y. Liu, M. H. Alkordi and M. Eddaoudi, *J*. *Am*. *Chem*. *Soc*., 2013, **135**, 7660-7667.

[13] K. Sumida, S. Horike, S. S. Kaye, Z. R. Herm, W. L. Queen, C. M. Brown, F. Grandjean, G. J. Long, A. Dailly and J. R. Long, *Chem. Sci.*, 2010, **1**, 184-191.

[14] C. Chen, W. Zhang, M. Zhang and J. Bai, *Inorg. Chem.*, 2019, **58**, 13836-13842.

[15] Q.-G. Zhai, Q. Lin, T. Wu, L. Wang, S.-T. Zheng, X. Bu and P. Feng, *Chem. Mater.*, 2012, **24**, 2624-2626.

[16] C. Chen, M. Zhang, W. Zhang and J. Bai, *Inorg. Chem.*, 2019, **58**, 2729-2735.

[17] H.-H. Wang, W.-J. Shi, L. Hou, G.-P. Li, Z. Zhu and Y.-Y. Wang, *Chem. Eur. J.*, 2015, **21**, 16525-16531.

[18] X. Song, M. Zhang, J. Duan and J. Bai, *Chem. Commun.*, 2019, **55**, 3477-3480.

[19] Y.-W. Li, H. Yan, T.-L. Hu, H.-Y. Ma, D.-C. Li, S.-N. Wang, Q.-X. Yao, J.-M. Dou, J. Xu and X.-H. Bu, *Chem. Commun.*, 2017, **53**, 2394-2397.

[20] M.-H. Choi, H. J. Park, D. H. Hong and M. P. Suh, *Chem. Eur. J.*, 2013, **19**, 17432-17438.

[21] J. Jiao, H. Liu, F. Chen, D. Bai, S. Xiong and Y. He, *Inorg. Chem. Front.*, 2016, **3**, 1411-1418.

[22] J. An and N. L. Rosi, *J. Am. Chem. Soc.*, 2010, **132**, 5578-5579.

[23] M. Y. Masoomi, K. C. Stylianou, A. Morsali, P. Retailleau and D. Maspoch, *Cryst. Growth Des.*, 2014, **14**, 2092-2096.

[24] C. E. Kivi, B. S. Gelfand, H. Dureckova, H. T. K. Ho, C. Ma, G. K. H. Shimizu, T. K. Woo and D. Song, *Chem. Commun.*, 2018, **54**, 14104-14107.

[25] J. Hu, T. Sun, X. Liu, Y. Guo and S. Wang, *RSC Adv.*, 2016, **6**, 64039-64046.

[26] X. Wu, B. Yuan, Z. Bao and S. Deng, *J. Colloid Interface Sci.*, 2014, 430, 78-84.

[27] L. Li, L. Yang, J. Wang, Z. Zhang, Q. Yang, Y. Yang, Q. Ren and Z. Bao, *AIChE J.*, 2018, **64**, 3681-3689.

[28] P.-Q. Liao, N.-Y. Huang, W.-X. Zhang, J.-P. Zhang and X.-M. Chen, *Science*, 2017, **356**, 1193.

[29] Y. Wang, N.-Y. Huang, J.-Q. Shen, P.-Q. Liao, X.-M. Chen and J.-P. Zhang, *J. Am. Chem. Soc.*, 2018, **140**, 38-41.

[30] S. Pérez-Yáñez, G. Beobide, O. Castillo, M. Fischer, F. Hoffmann, M. Fröba, J. Cepeda and A. Luque, *Eur. J. Inorg. Chem.*, 2012, **2012**, 5921-5933.

[31] G. Barin, V. Krungleviciute, D. A. Gomez-Gualdron, A. A. Sarjeant, R. Q. Snurr, J. T. Hupp, T. Yildirim and O. K. Farha, *Chem. Mater.*, 2014, **26**, 1912-1917.